THE JOURNAL OF PHYSICAL CHEMISTRY C

Article

pubs.acs.org/JPCC

Propane-d_6 Heterogeneously Hyperpolarized by Parahydrogen

Kirill V. Kovtunov,*[,†,‡,◆] Milton L. Truong,[§,◆] Danila A. Barskiy,[†,‡] Oleg G. Salnikov,[†,‡] Valery I. Bukhtiyarov,[¶] Aaron M. Coffey,[§,∥] Kevin W. Waddell,[§,⊥] Igor V. Koptyug,[†,‡] and Eduard Y. Chekmenev*[,§,∥,#,#]

[†]International Tomography Center, 3A Institutskaya St., Novosibirsk 630090, Russia

[‡]Novosibirsk State University, 2 Pirogova St., Novosibirsk, 630090, Russia

[§]Institute of Imaging Science, Department of Radiology, [∥]Department of Biomedical Engineering, [⊥]Department of Physics and Astronomy, [#]Department of Biochemistry, [#]Vanderbilt-Ingram Cancer Center, Vanderbilt University, Nashville, Tennessee 37232-2310, United States

[¶]Boreskov Institute of Catalysis, SB RAS, 5 Acad. Lavrentiev Pr., Novosibirsk 630090, Russia

ABSTRACT: Long-lived spin states of hyperpolarized propane-d_6 gas were demonstrated following pairwise addition of parahydrogen gas to propene-d_6 using heterogeneous parahydrogen-induced polarization (HET-PHIP). Hyperpolarized molecules were synthesized using Rh/TiO_2 solid catalyst with 1.6 nm Rh nanoparticles. Hyperpolarized ($P_H \sim 1\%$) propane-d_6 was detected at high magnetic field (9.4 T) spectroscopically and by high-resolution 3D gradient-echo MRI (4.7 T) as the gas flowed through the radiofrequency coil with a spatial and temporal resolution of 0.5 × 0.5 × 0.5 mm^3 and 17.7 s, respectively. Stopped-flow hyperpolarized propane-d_6 gas was also detected at 0.0475 T with an observed nuclear spin polarization of $P_H \sim 0.1\%$ and a relatively long lifetime with $T_{1,eff} = 6.0 \pm 0.3$ s. Importantly, it was shown that the hyperpolarized protons of the deuterated product obtained via pairwise parahydrogen addition could be detected directly at low magnetic field. Importantly, the relatively long low-field $T_{1,eff}$ of HP propane-d_6 gas is not susceptible to paramagnetic impurities as tested by exposure to ~0.2 atm oxygen. This long lifetime and nontoxic nature of propane gas could be useful for bioimaging applications including potentially pulmonary low-field MRI. The feasibility of high-resolution low-field 2D gradient-echo MRI was demonstrated with 0.88 × 0.88 mm^2 spatial and ~0.7 s temporal resolution, respectively, at 0.0475 T.

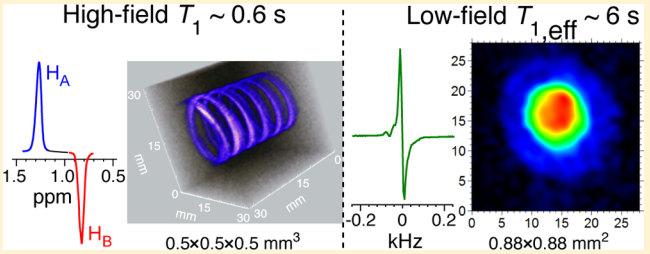

INTRODUCTION

While gas imaging is useful in studies of catalysis,[1] reactors,[2] porous media,[3,4] lungs,[5] etc.,[6] it is challenging due to the low molar concentrations of gases at normal pressure. Biomedical applications of gas imaging are of particular importance. For example, there is currently no widespread clinical imaging modality for functional lung imaging because computed tomography (CT), conventional MRI, and X-ray can only provide structural images of dense tissues[7]—e.g., tumors or pneumonia—but provide very little or no information about lung ventilation, perfusion, alveoli size, etc. Deadly diseases such as chronic obstructive pulmonary disease (COPD) with over 300 million people affected worldwide and ~3 million annual deaths do not have any imaging marker as of today.[8,9] This state of affairs contrasts with cancer imaging, which includes MRI, CT, ultrasound, mammography, positron emission tomography (PET), and others, which enable early detection via population screening and treatment response monitoring. High-sensitivity imaging techniques with low penetration depth such as fluorescence and other optical imaging approaches cannot be directly applied to lung imaging. Conversely, PET and MRI with molecular contrast agents have a relatively high penetration depth of tens of centimeters. Nuclear medicine approaches require a radioactive exogenous contrast agent such as ^{133}Xe gas or technetium-99m DTPA,[7] which enables lung imaging through visualization of inhaled gas. ^{133}Xe additionally enables brain imaging due to its ability to penetrate the blood-brain barrier. The disadvantages include the requirements for radioactive isotope handling and production and specialized imaging hardware, which result in a relatively high cost.

Conventional MRI unfortunately has a relatively low sensitivity for proton imaging of gases,[7] but two groups of inhalable contrast agents for heteronuclear NMR and MRI have been demonstrated to date. The first group is comprised of fluorinated gases. Perfluorinated carbon (PFC) compounds are used as inhalable contrast agents[10,11] which, once inhaled, can be imaged via the detection of the relatively NMR-sensitive ^{19}F stable isotope nucleus. Because there is virtually no ^{19}F NMR background signal *in vivo*, this method offers a very good contrast with the surrounding tissue. The main challenges of this method are (i) the relatively low spatial and especially

Received: August 28, 2014
Revised: November 6, 2014
Published: November 6, 2014

   dx.doi.org/10.1021/jp508719n | J. Phys. Chem. C 2014, 118, 28234−28243

temporal (minutes) resolution, caused by a low NMR signal-to-noise ratio (SNR) for the diluted PFC gases compared to tissue proton density, and (ii) the requirement for specialized hardware and MRI pulse sequences. The next group of methods relies on NMR hyperpolarization, which increases nuclear spin polarization by 4−6 orders of magnitude and more.[12−14] The spin exchange optical pumping (SEOP)[5] process hyperpolarizes noble gases including ^{3}He, ^{129}Xe, ^{131}Xe, and ^{83}Kr.[15] When inhaled, these hyperpolarized (HP) gases can be imaged by MRI on a single breath hold providing high-resolution 3D maps of lung perfusion, ventilation, apparent diffusion coefficient (ADC), and other lung-function-related metrics.[6,7,16−18] These hyperpolarization methods provide a great contrast between the lungs and other tissues because of the lack of background signal but require (i) highly specialized hyperpolarization equipment to create the hyperpolarized state and (ii) a multinuclear MRI scanner with a second RF detection channel in addition to the conventional proton RF channel. The above requirements limited these promising MRI imaging modalities for both PFC and HP noble gas contrast media to a few premier sites around the world.

An alternative to the fluorinated and the HP noble gas approaches is the use of proton HP contrast gas agents that can be detected using conventional proton MRI hardware and imaging sequences, which are already widely used in healthcare in developed and developing countries. While several hyperpolarization techniques have been developed to date, heterogeneous parahydrogen-induced polarization (HET-PHIP) is uniquely suited for the production of HP hydrocarbon gases at a solid−gas interface[19,20] because pure catalyst-free HP gases can be prepared in seconds using relatively simple low-cost hyperpolarization equipment.[1,21] Up to 1% HP propane gas was recently demonstrated, enabling 3D MRI with high spatial and temporal resolution under conditions of continuously flowing hyperpolarized gas.[22] While propane is a nontoxic asphyxiating gas, the biomedical use of HP propane as an MRI contrast agent applied via inhalation is hardly possible due to its short T_1 of ∼1 s.[23]

Most liquid-state PHIP agents significantly benefit from the increase in the PHIP yield and lifetime achieved upon deuteration of their molecular precursors.[13,24] Here, we investigate the utility of the deuterated propene precursor for the PHIP-based production of hyperpolarized propane-d_6 and its use in NMR at high and low magnetic fields. While deuteration is typically associated with significantly increased cost of chemical compounds (i.e., the use of propene-d_6 is inherently more expensive than the use of propene[22,25]), it should be pointed out that deuterated propene can be obtained via the process of deuterium exchange with D_2 or D_2O,[26,27] which will likely result in a relatively low cost of mass-produced propene-d_6 similar to that of D_2O.

It should also be noted that low-field MRI detection demonstrated here offers a potential advantage of improved sensitivity because low-field MRI can be more sensitive than high-field MRI for detection of hyperpolarized contrast media.[11,28] Moreover, irrespective of hyperpolarization, low-field MRI in general offers other advantages including (i) significantly reduced static magnetic susceptibility effects resulting in the reduced subject-induced B_0 inhomogeneities and (ii) a significantly reduced specific adsorption rate (SAR).[29] The latter advantages make low-field MRI a more robust, faster, and safer procedure in comparison to conventional high-field MRI.

Deuteration results in only a small increase in T_1 values of the HP product as demonstrated here by high-field NMR and MRI and thus provides little benefit in prolonging the hyperpolarization lifetime. However, the use of low magnetic fields allows the preparation of hyperpolarized long-lived spin states of the nascent pair of hydrogens of parahydrogen (p-H_2) after its pairwise addition to propene-d_6, and the significantly increased hyperpolarization lifetime is potentially suitable for biomedical imaging applications.

Propane is a nontoxic asphyxiant, and it has been shown to be nontoxic and safe in a long-term (90-day long) occupational exposure study at a concentration up to 10 000 ppm, which is below its lower explosive level (LEL) of 2.1%.[30] While additional toxicity studies may be required to warrant the safety of bolus inhalation of propane gas at significantly greater concentrations, the earlier work on long-term systemic exposure clearly advocates for propane being safe and nontoxic.[30] Moreover, the potential clinical translation will likely follow in the footsteps of hyperpolarized ^{129}Xe, which is a well-known anesthetic, and is now administered as a bolus inhalation contrast agent under high concentration of >50%. While propane is an explosive gas, it has a very low upper explosive level of ∼9.5%. Therefore, it can be potentially safely administered to humans for lung imaging at gas concentrations significantly exceeding its upper explosive limit (UEL) > 9.5%.

EXPERIMENTAL SECTION

Preparation of Gases for Hydrogenation Reactions. Ultrapure (>99.999%) hydrogen gas was used for the preparation of >90% p-H_2 using a previously described p-H_2 generator.[31] Propene-d_6 (99% atom D, Sigma-Aldrich 455687) and propene (Sigma-Aldrich 295663-300G) gases were used as supplied by the manufacturer without further purification. Gases were mixed immediately before their use in a custom mixing chamber, which represented a previously described[32,33] high-pressure ∼60 mL polysulfone reactor filled with plastic balls to yield the effective chamber volume of ∼30−60 mL. Propene-d_6 gas was filled in the chamber first, and the chamber was then filled with p-H_2 gas with ∼9.5 bar total pressure and a 1:2 ratio of propene-d_6:p-H_2 gases. Note that when propene gas is completely hydrogenated the resulting gas mixture consists of propane-d_6:p-H_2 in ∼1:1 ratio. Rh/TiO_2 catalyst (1.6 nm particle size) was described earlier.[22] Approximately 50 mg of this catalyst was packed inside an 1/8 in. OD copper tubing representing a variable-temperature (VT) reaction chamber.

9.4 T High-Resolution NMR Spectroscopy. High-resolution high-field NMR spectroscopy was conducted on a 9.4 T Bruker Avance NMR spectrometer. The experimental setups for ALTADENA[34] and PASADENA[35] experiments are presented in the corresponding figures. For ALTADENA experiments, the hydrogenation reaction was performed in a temperature-controlled reaction chamber at Earth magnetic field, and the resulting gas was transferred for detection to the 9.4 T NMR spectrometer via 1/16 in. OD (1/32 in. ID) Teflon tubing at a flow rate of 100 mL/min at 1 atm total gas pressure. HP gas was delivered to the bottom of a standard 5 mm NMR tube via 1/16 in. OD Teflon flexible tubing. The gas exited the NMR tube through an additional exhaust line (via 1/16 in. OD Teflon tubing) at the top of the NMR tube. For PASADENA experiments, a small quantity (a few milligrams) of Rh/TiO_2 catalyst was placed at the bottom of a standard 5 mm NMR tube, and the propene-d_6:p-H_2 mixture was delivered to the catalyst via 1/16 in. OD Teflon tubing. All experiments with

dx.doi.org/10.1021/jp508719n | J. Phys. Chem. C 2014, 118, 28234−28243

hydrogenation at Earth magnetic field were conducted at a reaction chamber temperature of ∼100 °C. While the gas stream leaves the reactor being very hot, the gas cools down rather rapidly because gases generally have relatively low thermal capacity and because the gas passes through a significant section (>1 m long) of 1/16 in. ID tubing. As a result, when the material is transferred to the 9.4 T magnet, it is already equilibrated to room temperature. This was additionally checked by blowing the stream of produced gases over the hand of the experimenter, and the gas was found to be cooled. The apparent enhancement factor ε(app,flow) was calculated by comparing the signal intensities of hyperpolarized (flow) and thermally polarized (stopped flow) gas samples using the method described earlier assuming that the HP gas already equilibrated to room temperature after passing though a very long section (>1 m) of tubing.[22] The rapid gas cool-down is a convenient and advantageous feature of this method for potential biomedical translation.

4.7 T 3D MRI. High-field 3D MRI studies were conducted using a 4.7 T Varian MRI scanner (Varian, Palo Alto, California) and a custom-built 38 mm ID dual-channel MRI coil tuned to ^{1}H frequency of 200.25 MHz. A 3D gradient echo MRI sequence (ge3D) was used for MRI with the following parameters: spectral width (SW) = 20 kHz, imaging matrix 64 × 64 × 64, field of view (FOV) = 32 × 32 × 32 mm^3, echo time (TE) = 2.2 ms, repetition time (TR) = 4.3 ms, voxel size 0.5 × 0.5 × 0.5 mm^3 (125 nL), RF excitation pulse angle (α) = 15° (500 μs, Gaussian shape) for HP propane-d_6 and α = 2° (500 μs, Gaussian shape) for the water phantom, total acquisition time of 17.7 s. No compressed sensing or other image acceleration technique was used, and no data manipulation was performed (i.e., zero-filling or smoothing). Percentage polarization of HP propane-d_6 gas was calculated as described earlier for HP propane gas and was estimated to be ∼1%.[22] It should be pointed out that this polarization estimate was done using spectroscopic detection of flowing HP propane with NMR FID of <100 ms.[22] This is important because the spectroscopic method provides a more reliable number because imaging of flowing propane gas at 4.7 T may suffer from significant MRI artifacts related to the fast flow and the encoding scheme.[22] A spiral-shaped phantom was prepared using Tygon (3/32 in. ID × 3/16 in. OD, McMaster Carr, Atlanta, GA, P/N 5552K22) tubing wrapped around a plastic syringe to provide the dimensionality for imaging studies. A constant HP gas flow rate (∼15 mL/min) was maintained during an entire 3D MRI scan.

0.0475 T NMR Spectroscopy and Nonslice-Selective 2D MRI. All low-field studies were carried out using a Kea2 NMR spectrometer (Magritek, Wellington, New Zealand) with a custom-built frequency optimized dual-channel RF ^{1}H-X probe.[28] The flow rate was not controlled in low-field MR experiments due to experimental limitations. Hyperpolarization via hydrogenation of propane-d_6 was conducted at Earth magnetic field, and HP gas was transferred into an ∼2 mL phantom (estimated transfer time <0.3 s) placed inside the 0.0475 T NMR magnet (Magritek, Wellington, New Zealand). HP propane-d_6 (or propane) gas was allowed to flow for ∼1 s time period, after which the flow was terminated, and the phantom chamber was filled with HP gas mixture (estimated 4.7 bar partial pressure of propane-d_6 (or propane) at ∼100 °C—unlike in high-field experiments, the exiting gas was passing through a very short section (<20 cm) of heated tubing) containing ∼150 mM HP propane-d_6 (or propane) corresponding to ∼300 μmol quantity. NMR HP spectroscopic signals of propane-d_6 and propane were referenced to the NMR signal from thermally polarized H_2O (2.8 g, ∼160 mmol, 55 M concentration, containing 5 mM $CuSO_4$). The enhancement factors ε were calculated by comparing the signal intensities and quantities of HP gas and thermally polarized reference sample of water as follows: $\varepsilon = (S_{HP} \times \chi_{H2O})/(S_{H2O} \times \chi_{HP}) \sim 6000$, where S_{HP} and S_{H2O} are the integrals of the NMR signals of HP propane-d_6 and water, respectively, and χ_{H2O} and χ_{HP} are molar quantities of water and HP propane-d_6, respectively. Percentage of proton polarization in HP propane-d_6 was computed using thermal equilibrium proton polarization at 0.0475 T of $P_H = 1.6 \times 10^{-7}$ or 1.6×10^{-5}% as follows: $P_{HP} = \varepsilon \times P_{THERMAL}$ yielding $P_{HP} \sim 0.1\%$ per each (two per molecule) hyperpolarized nascent proton. All NMR spectra were recorded using a 45° excitation rectangular shape RF pulse and one scan. A 2D MRI experiment was conducted using nonslice-selective 2D GRE sequence as supplied by the manufacturer (Magritek, Wellington, New Zealand) using the following pulse sequence parameters: TE/TR = 7.0/20 ms, acquisition time = 6.4 ms, SW = 5.0 kHz, RF excitation pulse (rectangular shape), α = 7° (6.0 μs), FOV = 28 × 28 mm^2 using 32 × 32 imaging matrix with two dummy scans with the total imaging time of ∼0.7 s. Imaging of HP propane-d_6 utilized a single average and was repeated every 3 s, while imaging of water utilized eight averages. All images from propane-d_6 utilized one average (NA), while images of water were recorded with NA = 8. All images were interpolated to 1024 × 1024 pixels via zero-filling the data to enhance visual representation.

Low-Field NMR Spectra Simulation. ^{1}H NMR spectra for propane, propane-d_6, and [3-^{13}C]propane were calculated based on the conventional spin-density matrix formalism. For propane, the following parameters were used: δ = 0.899 ppm (methyl, 6H), δ = 1.336 ppm (methylene, 2H), J_{HH} = 7.4 Hz. For ^{13}C-labeled propane, $\delta(^{13}C)$ = 16.2 ppm and $^1J_{CH}$ = 125 Hz were used, with the two H atoms inherited from parahydrogen residing on the two unlabeled (^{12}C) carbons in the propane molecule. For propane-d_6, the vicinal couplings were $^3J_{HH}$ = 7.4 Hz, $^3J_{HD}$ = 1.12 Hz, and $^3J_{DD}$ = 0.17 Hz, while for the geminal H−D couplings the value $^2J_{HD}$ = 2 Hz was used.

Evolution of spin density matrix in the external magnetic field was evaluated by diagonalizing the Hamiltonian matrix to find eigenstates and eigenenergies of the spin system. The spin density matrix was then converted to the eigenbasis, and its elements were propagated in time using the respective differences in eigenenergies. Evolution under the action of hard pulses was evaluated by constructing and applying the corresponding rotation operators, with only ^{1}H nuclei affected by the pulses. Two types of calculations were performed: (1) assuming that both reaction and NMR signal detection took place at the 0.0475 T field and (2) for reaction performed at the Earth's field followed by adiabatic sample transfer to 0.0475 T for NMR signal detection. The calculation results were found to be almost identical. The field sweep was incorporated, when required, by using a series of short free evolution intervals interleaved with small stepwise increments in the magnetic field. The number of intervals (100−1000) was increased until no further changes in the calculated spectra were observed. The FID was calculated based on the free evolution of the density matrix with periodic calculation of transverse magnetization for ^{1}H nuclei, followed by Fourier transform to generate the spectrum. Relaxation effects were not included in the calculations.

dx.doi.org/10.1021/jp508719n | J. Phys. Chem. C 2014, 118, 28234−28243

RESULTS AND DISCUSSION

The conventional ALTADENA[34] experiment relies on the pairwise addition of p-H_2 to an unsaturated precursor in a very low magnetic field under conditions of $\gamma_H B_0(\delta(H_A) - \delta(H_B))/2\pi \ll J_{HA\text{-}HB}$, which is followed by a rapid yet adiabatic sample transfer to a high-field NMR spectrometer and detection of the dissociated singlet of nascent parahydrogen protons under conditions of $\gamma_H B_0(\delta(H_A) - \delta(H_B))/2\pi \gg J_{HA\text{-}HB}$, where $\gamma_H B_0(\delta(H_A) - \delta(H_B))/2\pi$ is the chemical shift difference (in units of Hz) of the two nascent protons H_A and H_B (Figure 1b). The resulting ALTADENA spectrum (Figure 1d) of HP propane-d_6 shows the expected two NMR lines corresponding to H_A and H_B protons of propane-d_6 gas with the signal enhancement ε(app,flow) = 100 ± 5 (measured by comparison with the thermal spectrum of stopped gas, Figure 1e; the signal enhancement is similar to that observed for nondeuterated propane under similar experimental conditions).[22]

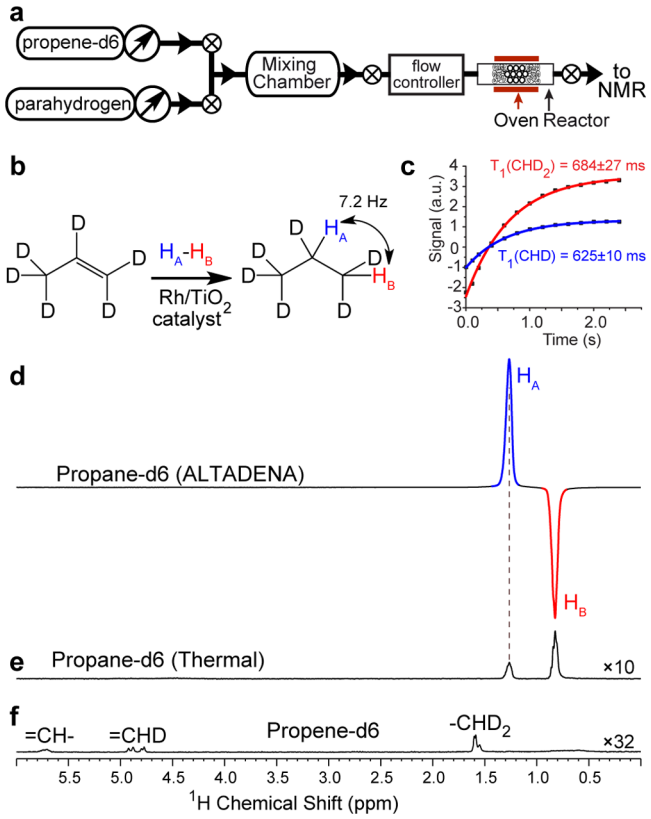

Figure 1. ALTADENA single-scan NMR spectroscopy of HP propane-d_6 with detection at 9.4 T: (a) experimental setup diagram, (b) the diagram of pairwise addition of p-H_2 (shown as $H_A - H_B$) to propene-d_6 resulting in propane-d_6, (c) T_1 measurements for thermally polarized propane-d_6 by the inversion−recovery method[36] at 9.4 T, (d) ALTADENA spectrum of HP propane-d_6 with ε(app,flow) = 100 ± 5 with respect to the spectrum (e) of stopped thermally polarized propane-d_6 gas, where unequal thermal resonances for CHD and CD_2H protons are formed due to fast H−D exchange reaction over the metal surface of heterogeneous catalyst, and (f) 32-scan spectrum of thermally polarized propene-d_6 gas showing residual ^{1}H proton signals in propene-d_6 groups.

While deuteration may increase T_1, this effect was found to be very minor at 9.4 T. For example, T_1 (CHD_2−) is 684 ± 27 ms vs T_1 (CH_3−) = 616 ± 16 ms, and T_1 (−CHD−) is 625 ± 10 ms vs T_1 (−CH_2−) = 532 ± 6 ms, in propane-d_6 and propane, respectively. These relatively low T_1 values present an experimental challenge for the detection of HP gas because of the relaxation losses during gas transport from the reactor to the NMR detector (Figure 1a). Moreover, short T_1 is a fundamental barrier for potential biomedical translation of HP propane (and other HP hydrocarbons) as an inhalable HP contrast agent for pulmonary imaging in a manner similar to HP ^{129}Xe[6,7] and other HP noble gases.

Despite the limitations associated with a relatively short T_1, HP propane gas can be successfully used for high-resolution hyperpolarized imaging. An example of high-resolution 3D MRI is provided in Figure 2a, where a spiral-shaped phantom was filled with the flowing HP propane-d_6 gas. The MR image with 0.5 × 0.5 × 0.5 mm^3 spatial and 17.7 s temporal resolution is demonstrated using polarization levels of $P_H \sim 1\%$ for HP propane-d_6 gas. A corresponding image of thermally polarized water is provided in Figure 2b. The SNR of 3D images of HP propane-d_6 gas and water were similar, demonstrating that proton images of hyperpolarized gases can be obtained with a quality similar to that of water. The clear advantages of proton hyperpolarized gas (vs ^{129}Xe[6,7,37] or other hyperpolarized noble gases) such as propane-d_6 shown here include the use of widely available proton-detecting imaging hardware and conventional and advanced[38] fast 3D proton MRI sequences. For example, the images presented in Figure 2a were acquired using a conventional 3D GRE MRI sequence as supplied by the MRI instrument manufacturer. It should also be noted that the images presented in Figure 2a have an approximately 2-fold better spatial resolution (as measured by the voxel size) compared to 0.625 × 0.625 × 0.625 mm^3 spatial resolution demonstrated earlier with HP nondeuterated propane.[22]

Moreover, the fully deuterated unsaturated substrate propene-d_6 enables the studies of the hydrogenation reaction mechanism via the *in situ* detection of HP products through PASADENA[35] protocol, where heterogeneous hydrogenation is carried out inside a 5 mm NMR tube with the *in situ* NMR signal detection[39,40] (Figure 3a). While the PASADENA spectrum of HP propane-d_6 produced via pairwise addition of p-H_2 primarily consists of two antiphase NMR lines corresponding to two nascent protons H_A and H_B derived from the p-H_2 molecule (Figure 3b), there are additional enhanced NMR signals, which correspond to HP propene. It should be noted that propene-d_6 (99% labeling with deuterium) carries essentially no protons, while Figure 4b clearly illustrates the enhanced antiphase resonances 3, 4, 5, and 6 of partially deuterated propenes with PASADENA hyperpolarized protons. These observations suggest that these resonances correspond to nascent protons derived from p-H_2 via (i) pairwise addition to propene-d_6 followed by subsequent dehydrogenation (loss of D_2) (Figure 4a) or via an alternative pathway of (ii) propene-d_6 dehydrogenation followed by pairwise addition of p-H_2 to propyne-d_4. While both pathways are possible, the second pathway is either nonexistent or has a minor contribution because it cannot produce the HP resonance 4 clearly seen in Figure 4. Note that nonpairwise H_2 addition is the major reaction mechanism accounting for most (>95%[23]) of the produced propane, and most parahydrogen-derived spin order is lost due to the dominance of the nonpairwise reaction mechanism and relaxation, i.e., only up to 1% is retained on the propane spin ensemble of nascent parahydrogen protons. Nevertheless, the nonpairwise route (i.e., without preservation of p-H_2 derived hyperpolarization) also involves the H/D exchange process described in Figure 4a on the surface of Rh/

dx.doi.org/10.1021/jp508719n | J. Phys. Chem. C 2014, 118, 28234−28243

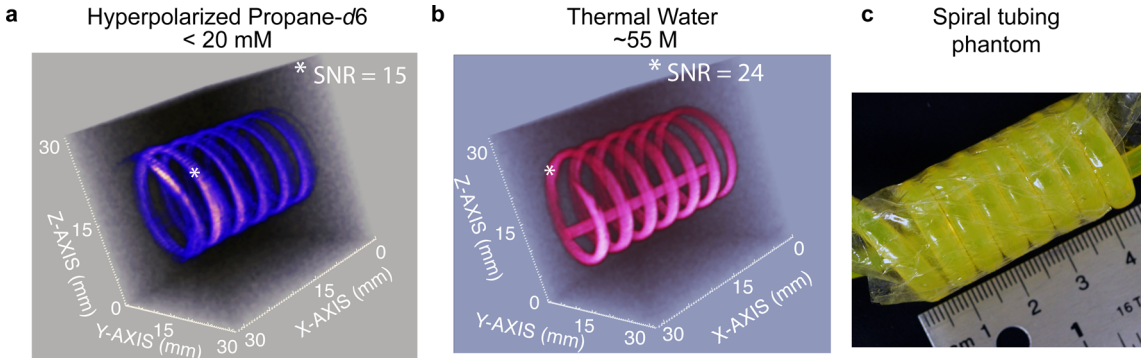

Figure 2. High-resolution 3D gradient echo (GRE) MRI at 4.7 T. (a) 3D MRI of flowing ~20 mM HP propane gas with 0.5 × 0.5 × 0.5 mm^3 spatial and 17.7 s temporal resolution with 32 × 32 × 32 mm^3 field of view. (b) The corresponding image of still thermally polarized 55 M tap water and (c) photograph of spiral phantom used for MRI imaging studies shown in (a) and (b). Signal-to-noise ratio (SNR) values are provided for representative voxels marked with white asterisk (*).

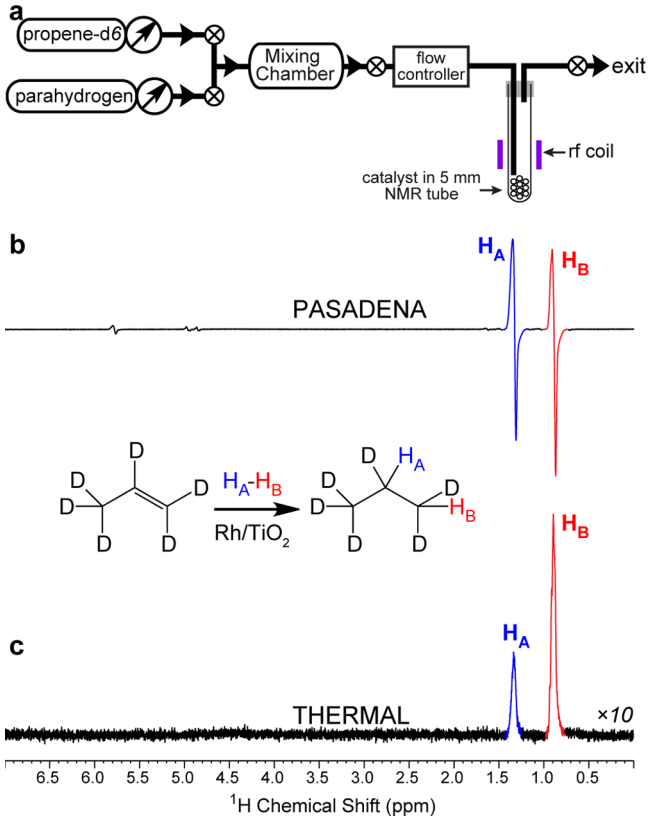

Figure 3. PASADENA NMR spectroscopy of HP propane-d_6 with detection at 9.4 T: (a) experimental setup diagram, (b) PASADENA spectrum (8 averages) of HP propane-d_6, and (c) 32-scan spectrum of thermally polarized propane-d_6 gas. The inset scheme shows pairwise addition of p-H_2 (shown as H_A − H_B) to propene-d_6 resulting in propane-d_6.

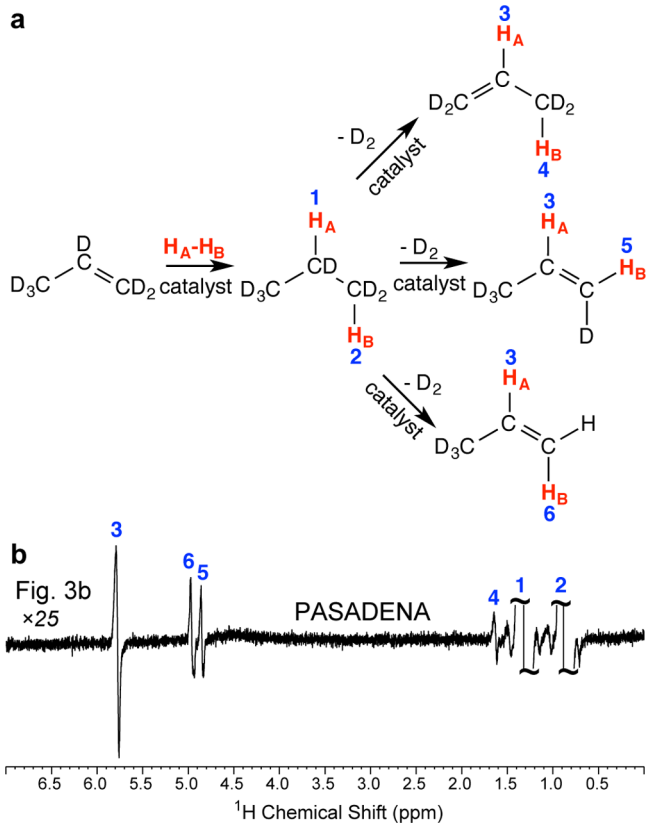

Figure 4. Reaction mechanism of pairwise addition of p-H_2 to propene-d_6 and dehydrogenation leading to the observation of PASADENA signals in partially deuterated propenes: (a) pathways of hydrogenation/dehydrogenation reactions leading to incorporation of p-H_2 (shown as H_A − H_B) into partially deuterated propenes and (b) scaled (×25) spectrum shown in Figure 3b.

TiO_2 catalyst because the signal ratio of methyl and methylene peaks is far from 1:1 (which would be expected if only one p-H_2 molecule were incorporated in one propene-d_6 molecule) as seen in the thermally polarized spectrum (Figure 1e) of hydrogenated gas. This indicates that on average more than two protons are being incorporated in the final hydrogenated product, which strictly speaking should not be referred to as propane-d_6.

Moreover, these mechanistic studies indicate that enhanced resonances 3, 4, 5, and 6 are derived through p-H_2 addition and dehydrogenation processes rather than through other mechanisms of polarization transfer from p-H_2. In contrast, if normal (i.e., nondeuterated) propene was used in the above PASADENA studies, it would be difficult to elucidate the mechanism of formation of HP propene species. Therefore, the deuterated precursor is an important and unique tool for mechanistic studies of hydrogenation processes.

Furthermore, NMR and MRI detection can be performed at low magnetic fields.[41−43] In addition, the detection efficiency of HP NMR and MRI (defined as SNR) in low magnetic fields

dx.doi.org/10.1021/jp508719n | J. Phys. Chem. C 2014, 118, 28234−28243

can in fact significantly exceed that of high-field HP detection.[28,32,33] Low-field NMR can offer the regime of a strongly coupled spin system with $\gamma_H B_0(\delta(H_A) - \delta(H_B))/2\pi < J_{HA\text{-}HB}$, and therefore the singlet spin state of the nascent protons derived from p-H_2 may remain partially associated. NMR detection of HP propane-d_6 obtained using the setup shown in Figure 5a enabled NMR detection at 0.0475 T,[32,33]

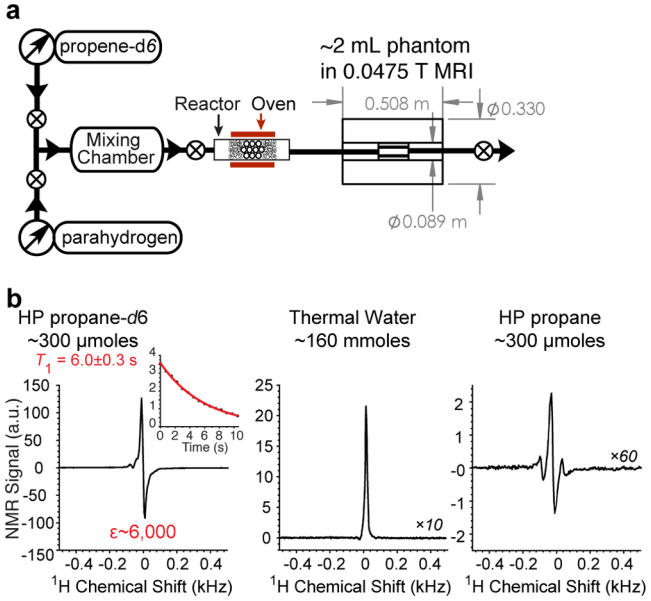

Figure 5. Stopped-flow NMR spectroscopy of hyperpolarized propane-d_6 gas at 0.0475 T. (a) Experimental setup diagram and (b) (left) single-scan NMR spectrum of HP propane-d_6 after pairwise addition of p-H_2 to propene-d_6 in Earth magnetic field. The inset shows the decay of HP signal measured with a small-angle RF excitation pulse (α = 7°); (middle) the corresponding spectrum of thermally polarized water, and (right) the corresponding spectrum of HP propane. It should be noted that the effect of 7° RF excitation pulse on magnetization is negligible (>99% of residual polarization is retained after each RF pulse) conveniently allowing *in situ* direct monitoring of exponential signal decay, i.e., T_1 measurement.[32,37,44]

where $\gamma_H B_0(\delta(H_A) - \delta(H_B))/2\pi$ of ~1 Hz is significantly smaller than $J_{HA\text{-}HB}$ of ~7 Hz. The spectroscopic NMR detection of stopped HP propane-d_6 gas (Figure 5b) revealed a strongly enhanced signal with ε(app,stopped) ~ 6000 corresponding to P_H ~ 0.1% (per nascent proton) by referencing the NMR signal of thermally polarized water. Experimentations with nondeuterated HP propane under identical experimental conditions (Figure 5b) revealed a significant collapse of the NMR signal due to a small chemical shift difference between H_A and H_B.

Theoretical simulations of the experiments intended to verify the observed significant difference in the NMR signals of deuterated and nondeuterated propane were performed (Figure 6). The very large difference between signal enhancements for propane and propane-d_6 can be rationalized as follows. At the magnetic field of 0.0475 T, the methyl and methylene proton spins of propane are strongly coupled and essentially represent a system of eight almost magnetically equivalent spins. In the reaction of propene with p-H_2, the numerous spin states of propane are populated in such a way that the allowed NMR transitions correspond to very small spin level population differences and thus give very weak signals, whereas significant population differences created by the reaction correspond to

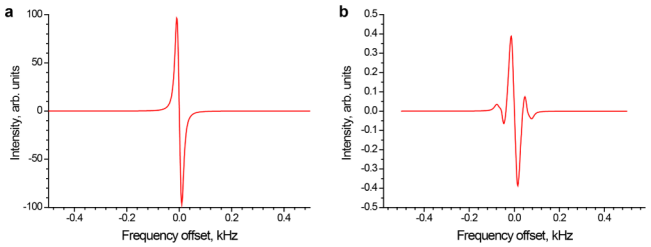

Figure 6. Calculated ^{1}H NMR spectra of HP propane and its isotopomers after pairwise addition of p-H_2 to corresponding propenes in a chemical reaction performed at 0.0475 T magnetic field. (a) The spectrum calculated for propane-d_6. (b) The weighted sum of the spectra of propane and [3-^{13}C]propane (it is assumed that the two hydrogen atoms inherited from p-H_2 are in positions 1 and 2 in the propane molecule). The contribution of [3-^{13}C]propane was multiplied by 0.011 to take into account ^{13}C natural abundance. Note the different vertical scales for the two spectra.

transitions which are normally forbidden. In terms of a two-spin system, this would correspond to small population differences within the manifold of the NMR-active triplet spin state and a large population difference between the singlet and triplet manifolds which gives no observable NMR signal. However, because the two chemical shifts are unequal, mixing of the triplet and singlet states makes the nominally forbidden transitions slightly allowed, which, combined with the large population difference between the singlet and triplet manifolds, leads to the observation of a moderate intensity spectrum. We note that for an eight-spin system, this "singlet−triplet" terminology is applicable only in qualitative terms, but it is still quite illustrative. For propane-d_6, the presence of deuterium atoms removes the near-magnetic equivalence of the two H atoms inherited by propane from p-H_2, and the corresponding mixing of spin states ensures that large population differences are now associated with fully allowed transitions, leading to much larger signal intensity in the observed NMR spectrum (Figure 6).

The polarization decay time measurements for HP propane-d_6 yielded a value of $T_{1,eff}$ = 6.0 ± 0.3 s (Figure 5b inset), which is an order of magnitude greater than the high-field T_1 value of ~0.6 s. Furthermore, the addition of 0.2 atm of O_2 introduced to HP propane-d_6 did not affect its $T_{1,eff}$ of ~6 s. The increase in T_1 (and its insensitivity to paramagnetic O_2 impurity) is highly desirable because it renders the opportunity to use HP propane gas for biomedical applications as a potential inhalable proton hyperpolarized contrast agent.

This effect of creation of longer-lived large population differences between the spin states of nascent p-H_2 proton spins is likely to be universal for PHIP (and potentially other HP methods), and we term it Nuclear Alignment of Spin Hyperpolarization via Interactions in Long-lived Low-field Ensembles (NASHVILLE) to make distinction with PASADENA and ALTADENA conditions. A number of perdeuterated PHIP precursors similar to propene-d_6 employed here are already available for efficient, i.e., resulting in near unity, hyperpolarization. These precursors can be used for PHIP of HEP for MRI angiography,[45] TFPP for coronary plaque imaging,[46] succinate[47,48] for cancer imaging,[49] phospholactate,[13,50] and propargylcholine.[51] It can be speculated that they are good candidates for NASHVILLE experiments to achieve long-lived ^{1}H spin states in low magnetic field without the requirement for the polarization transfer from nascent protons to ^{13}C or ^{15}N heteronucleus.[52−55]

dx.doi.org/10.1021/jp508719n | J. Phys. Chem. C 2014, 118, 28234−28243

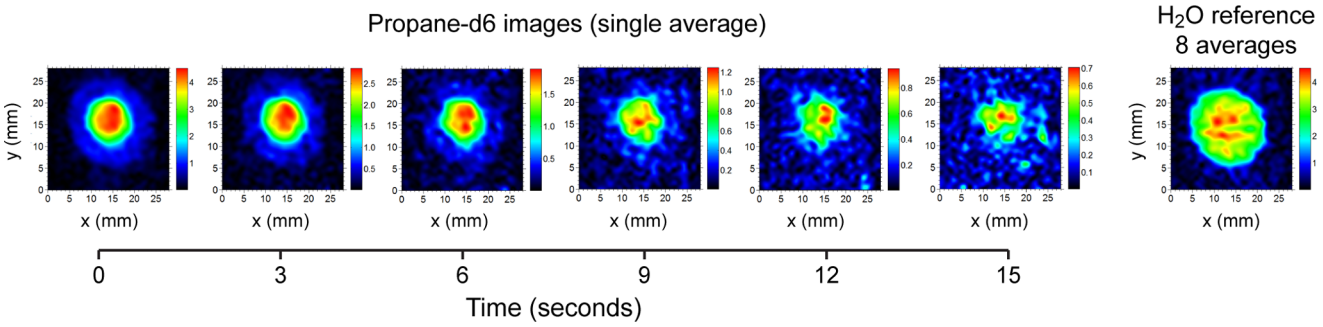

Figure 7. Subsecond single-average nonslice-selective 2D MRI of 150 mM HP propane-d_6 (~2 mL volume) at 0.0475 T with 0.88 × 0.88 mm^2 spatial and ~0.7 s temporal resolution with 28 × 28 mm^2 field of view. The same batch of HP propane was used for subsequent 2D MRI scans every 3 s. Note that propane-d_6 images are more intense in the center due to greater sample depth in the center of the phantom variable cylindrical shape. The image on the right shows the corresponding 2D image (8 averages) of 55 M thermally polarized water (~2.8 mL volume).

The increase of the lifetime of the HP state of propane-d_6 at low magnetic field through creation of long-lived states is hardly surprising because a significant increase in singlet lifetime vs conventional T_1 was demonstrated in seminal works by Levitt,[56,57] Warren,[58,59] and others.[60] While T_1 of HP propane-d_6 (~6 s) is relatively low, it exceeds that of HP ^{83}Kr,[61] and it is certainly sufficiently long to enable *in vivo* administration via inhalation.

Low-field MRI has a potential for biomedical application of HP propane-d_6 described above, and the feasibility of subsecond low-field MRI is successfully demonstrated in Figure 7. 2D (without slice selection) GRE MRI images were acquired with submillimeter (0.88 × 0.88 mm^2 pixel size) spatial resolution in ~0.7 s. The repetition time (TR = 20 ms) was limited by the electronics response and can be significantly accelerated in the future similarly to the GRE MRI (TR = 4.3 ms) presented in Figure 2a. Furthermore, shorter TR can also potentially enable sufficiently high scan speed required for 3D imaging of HP gas.[37,62]

The level of signal enhancement ($\varepsilon \sim 6000$) enabled higher SNR in the images of HP propane compared to that of thermally polarized water (Figure 7). This is important because potential *in vivo* direct proton imaging of this HP contrast agent will have to consider the background signal from water in the surrounding tissue.[63,64] Moreover, the available P_H was only 0.1% at 0.0475 T. Further improvements to achieve higher P_H values are possible for boosting the imaging SNR, which would improve the dominance of the HP propane-d_6 signal over the thermal water background.

A significant discrepancy between the apparent P_H values for HP propane-d_6 at high and low magnetic fields (~1% and 0.1%, respectively) can be explained by (i) the difference in experimental setup (experiments at high field utilized constant gas flow, whereas low-field experiments lacked flow control) and (ii) additional relaxation losses in low-field experiments because HP gas was stopped first, causing an additional time delay (~2−3 s). Moreover, partial collapse of an antiphase NMR peak due to B_0 field inhomogeneities cannot be completely ruled out.[65] Furthermore, the possibility of incorporation of more than one pair of p-H_2 into the final product via a pairwise route cannot be ruled out (see discussion regarding the mechanism of H/D exchange above), and extra protons may cause collapse of the NMR line similarly to that shown in Figures 5b and 6b for natural abundance propane.

HP propane-d_6 gas was prepared within seconds via heterogeneous catalytic hydrogenation. While a relatively small production quantity (a few milliliters) of HP propane-d_6 was demonstrated, there are no fundamental barriers for scaling it up to a clinically relevant dose of ~1 L. Despite a relatively low percentage polarization (0.1−1%) achieved for propane to date,[22] it should be pointed out that each HP propane molecule carries a payload of two hyperpolarized protons compared to monatomic hyperpolarized ^{129}Xe. Furthermore, protons have a ~3.6-fold greater gyromagnetic ratio and a ~4-fold greater natural abundance compared to those of ^{129}Xe. The combination (calculated as a product) of these factors makes HP propane ~40 times more sensitive compared to ^{129}Xe at the same polarization level. Furthermore, the process of SEOP of noble gases is time-consuming, whereas HP propane-d_6 can be prepared on demand, which can additionally enable signal averaging to improve SNR through potentially multiple inhalations of HP propane-d_6. Nevertheless, the recent technological[44,66−69] and fundamental[14,37] advances[70] in SEOP hyperpolarization of ^{129}Xe enabled ^{129}Xe polarization to approach order unity (i.e., →100%). Therefore, despite nominally better detection sensitivity of propane vs ^{129}Xe, further improvements in hyperpolarization level of HP propane are required to truly enable better detection sensitivity of HP propane-d_6 vs HP ^{129}Xe in addition to the other two realized benefits of (i) direct proton detection enabling MRI imaging on widely available proton MRI scanners and (ii) the relative ease and cost (of hyperpolarization equipment) of HP propane-d_6 production.

An additional benefit of HP propane is the use of proton NMR detection, which is universally available unlike detection of ^{129}Xe, ^{13}C, and ^{3}He requiring multinuclear detection capability.[71,72] The main limitation of the described use of HP propane-d_6 at 0.0475 T is the prerequisite of low-field MRI scanners, which are less widespread than conventional high-field MRI scanners. However, it should be pointed out that low-field HP MRI[62,73,74] can be more sensitive than HP high-field MRI[28] making the low-field MRI a very well-suited molecular imaging modality. Moreover, specific adsorption rate (SAR) is negligible at low resonance frequencies,[29] which provides fewer limitations (for example, SAR can limit the speed of MRI scan) and an increased patient safety.

■ CONCLUSIONS

Propene-d_6 gas was efficiently hyperpolarized using the HET-PHIP technique and Rh/TiO_2 catalyst allowing for preparation of pure (from catalyst) HP propane-d_6 gas. While deuteration of the propene precursor was not effective for increasing T_1 at

dx.doi.org/10.1021/jp508719n | J. Phys. Chem. C 2014, 118, 28234−28243

9.4 T, it nevertheless demonstrates a number of advantages compared to unlabeled propene. PHIP of propane-d_6 provides significant advantages for the mechanistic studies of the catalytic hydrogenation reaction, showing in particular that propene gas is hydrogenated to yield propane, which can be subsequently dehydrogenated by the catalyst studied. Propene-d_6 can also be useful for high-resolution high-field MRI of flowing HP propane-d_6 gas as demonstrated here by 3D MRI with 0.5 × 0.5 × 0.5 mm^3 and 17.7 s spatial and temporal resolution.

Low-field NMR at 0.0475 T enabled efficient direct detection of PHIP hyperpolarized propane-d_6 in contrast to non-deuterated PHIP polarized propane. The longer-lived low-field ensembles (NASHVILLE effect) additionally allow for a significant (factor of ∼10) increase in hyperpolarization decay time. This new approach can potentially be extended to other perdeuterated precursors suitable for PHIP hyperpolarization. The feasibility of multiscan low-field MRI was demonstrated with the spatial and temporal resolution of 0.88 × 0.88 mm^2 (pixel size) and ∼0.7 s, respectively. Multiple subsecond MR images were recorded on a single batch of stopped-flow HP propane-d_6 gas during an ∼15 s long time window. The feasibility of high-resolution MRI should pave the way to biomedical use of PHIP hyperpolarized propane-d_6 as an inhalable contrast agent for pulmonary imaging using proton MRI hardware and pulse sequences.

AUTHOR INFORMATION

Corresponding Authors

*E-mail: kovtunov@tomo.nsc.ru.

*E-mail: eduard.chekmenev@vanderbilt.edu.

Author Contributions

◆These authors contributed equally.

Notes

The authors declare no competing financial interest.

ACKNOWLEDGMENTS

KVK and IVK thank RSCF (14-35-00020) grant for supporting the work on the gaseous contrast agents' production. OGS, DAB, and VIB thank RSCF (14-13-00445) grant for support of catalyst preparation and its tests. IVK also thanks RFBR (14-03-93183 MCX_a) grant for supporting the work on low-field NMR spectra simulation. US team thanks NIH ICMIC 5P50 CA128323-03, 5R00 CA134749-03, 3R00CA134749-02S1, NIH 1R21EB018014, NSF CHE-1416268, and DoD CDMRP Breast Cancer Program Era of Hope Award W81XWH-12-1-0159/BC112431 for support of MRI and NMR experiments performed at Vanderbilt University.

REFERENCES

(1) Bouchard, L. S.; Burt, S. R.; Anwar, M. S.; Kovtunov, K. V.; Koptyug, I. V.; Pines, A. NMR Imaging of Catalytic Hydrogenation in Microreactors with the Use of Para-Hydrogen. *Science* **2008**, *319*, 442−445.

(2) Lysova, A. A.; Koptyug, I. V. Magnetic Resonance Imaging Methods for in Situ Studies in Heterogeneous Catalysis. *Chem. Soc. Rev.* **2010**, *39*, 4585−4601.

(3) Meersmann, T.; Logan, J. W.; Simonutti, R.; Caldarelli, S.; Comotti, A.; Sozzani, P.; Kaiser, L. G.; Pines, A. Exploring Single-File Diffusion in One-Dimensional Nanochannels by Laser-Polarized Xe-129 NMR Spectroscopy. *J. Phys. Chem. A* **2000**, *104*, 11665−11670.

(4) Koptyug, I. V. MRI of Mass Transport in Porous Media: Drying and Sorption Processes. *Prog. Nucl. Mag. Reson. Spectrosc.* **2012**, *65*, 1−65.

(5) Walker, T. G.; Happer, W. Spin-Exchange Optical Pumping of Noble-Gas Nuclei. *Rev. Mod. Phys.* **1997**, *69*, 629−642.

(6) Goodson, B. M. Nuclear Magnetic Resonance of Laser-Polarized Noble Gases in Molecules, Materials, and Organisms. *J. Magn. Reson.* **2002**, *155*, 157−216.

(7) Mugler, J. P.; Altes, T. A. Hyperpolarized ^{129}Xe MRI of the Human Lung. *J. Magn. Reson. Imaging* **2013**, *37*, 313−331.

(8) Qing, K.; Mugler, J. P.; Altes, T. A.; Jiang, Y.; Mata, J. F.; Miller, G. W.; Ruset, I. C.; Hersman, F. W.; Ruppert, K. Assessment of Lung Function in Asthma and COPD Using Hyperpolarized ^{129}Xe Chemical Shift Saturation Recovery Spectroscopy and Dissolved-Phase MRI. *NMR Biomed.* **2014**, DOI: 10.1002/nbm.3179.

(9) Ouriadov, A.; Farag, A.; Kirby, M.; McCormack, D. G.; Parraga, G.; Santyr, G. E. Lung Morphometry Using Hyperpolarized ^{129}Xe Apparent Diffusion Coefficient Anisotropy in Chronic Obstructive Pulmonary Disease. *Magn. Reson. Med.* **2013**, *70*, 1699−1706.

(10) Jacob, R. E.; Chang, Y. V.; Choong, C. K.; Bierhals, A.; Hu, D. Z.; Zheng, J.; Yablonskiy, D. A.; Woods, J. C.; Gierada, D. S.; Conradi, M. S. F-19 MR Imaging of Ventilation and Diffusion in Excised Lungs. *Magn. Reson. Med.* **2005**, *54*, 577−585.

(11) Conradi, M. S.; Saam, B. T.; Yablonskiy, D. A.; Woods, J. C. Hyperpolarized He-3 and Perfluorocarbon Gas Diffusion MRI of Lungs. *Prog. Nucl. Mag. Reson. Spectrosc.* **2006**, *48*, 63−83.

(12) Ardenkjaer-Larsen, J. H.; Fridlund, B.; Gram, A.; Hansson, G.; Hansson, L.; Lerche, M. H.; Servin, R.; Thaning, M.; Golman, K. Increase in Signal-to-Noise Ratio of > 10,000 Times in Liquid-State Nmr. *Proc. Natl. Acad. Sci. U.S.A.* **2003**, *100*, 10158−10163.

(13) Shchepin, R. V.; Coffey, A. M.; Waddell, K. W.; Chekmenev, E. Y. Parahydrogen Induced Polarization of 1-^{13}C-Phospholactate-D2 for Biomedical Imaging with >30,000,000-Fold NMR Signal Enhancement in Water. *Anal. Chem.* **2014**, *86*, 5601−5605.

(14) Nikolaou, P.; Coffey, A. M.; Barlow, M. J.; Rosen, M.; Goodson, B. M.; Chekmenev, E. Y. Temperature-Ramped ^{129}Xe Spin Exchange Optical Pumping. *Anal. Chem.* **2014**, *86*, 8206−8212.

(15) Lilburn, D.; Pavlovskaya, G. E.; Meersmann, T. Perspectives of Hyperpolarized Noble Gas MRI Beyond ^{3}He. *J. Magn. Reson.* **2012**, *229*, 173−186.

(16) Muradyan, I.; Butler, J. P.; Dabaghyan, M.; Hrovat, M.; Dregely, I.; Ruset, I.; Topulos, G. P.; Frederick, E.; Hatabu, H.; Hersman, W. F.; et al. Single-Breath Xenon Polarization Transfer Contrast (SB-XTC): Implementation and Initial Results in Healthy Humans. *J. Magn. Reson. Imaging* **2013**, *37*, 457−470.

(17) Mugler, J. P.; Altes, T. A.; Ruset, I. C.; Dregely, I. M.; Mata, J. F.; Miller, G. W.; Ketel, S.; Ketel, J.; Hersman, F. W.; Ruppert, K. Simultaneous Magnetic Resonance Imaging of Ventilation Distribution and Gas Uptake in the Human Lung Using Hyperpolarized Xenon-129. *Proc. Natl. Acad. Sci. U.S.A.* **2010**, *107*, 21707−21712.

(18) Dregely, I.; Ruset, I. C.; Mata, J. F.; Ketel, J.; Ketel, S.; Distelbrink, J.; Altes, T. A.; Mugler, J. P.; Miller, G. W.; Hersman, F. W.; et al. Multiple-Exchange-Time Xenon Polarization Transfer Contrast (MXTC) MRI: Initial Results in Animals and Healthy Volunteers. *Magn. Reson. Med.* **2012**, *67*, 943−953.

(19) Kovtunov, K. V.; Beck, I. E.; Bukhtiyarov, V. I.; Koptyug, I. V. Observation of Parahydrogen-Induced Polarization in Heterogeneous Hydrogenation on Supported Metal Catalysts. *Angew. Chem., Int. Ed.* **2008**, *47*, 1492−1495.

(20) Kovtunov, K. V.; Barskiy, D. A.; Salnikov, O. G.; Khudorozhkov, A. K.; Bukhtiyarov, V. I.; Prosvirin, I. P.; Koptyug, I. V. Parahydrogen-Induced Polarization (PHIP) in Heterogeneous Hydrogenation over Bulk Metals and Metal Oxides. *Chem. Commun.* **2014**, *50*, 875−878.

(21) Bouchard, L. S.; Kovtunov, K. V.; Burt, S. R.; Anwar, M. S.; Koptyug, I. V.; Sagdeev, R. Z.; Pines, A. Para-Hydrogen-Enhanced Hyperpolarized Gas-Phase Magnetic Resonance Imaging. *Angew. Chem., Int. Ed.* **2007**, *46*, 4064−4068.

(22) Kovtunov, K. V.; Barskiy, D. A.; Coffey, A. M.; Truong, M. L.; Salnikov, O. G.; Khudorozhkov, A. K.; Inozemceva, E. A.; Prosvirin, I.

P.; Bukhtiyarov, V. I.; Waddell, K. W.; et al. High-Resolution 3D Proton Hyperpolarized Gas Mri Enabled by Parahydrogen and Rh/TiO_2 Heterogeneous Catalyst. *Chem.—Eur. J.* **2014**, *20*, 11636−11639.
(23) Kovtunov, K. V.; Zhivonitko, V. V.; Skovpin, I. V.; Barskiy, D. A.; Koptyug, I. V. Parahydrogen-Induced Polarization in Heterogeneous Catalytic Processes. *Top. Curr. Chem.* **2013**, *338*, 123−180.
(24) Shchepin, R. V.; Coffey, A. M.; Waddell, K. W.; Chekmenev, E. Y. PASADENA Hyperpolarized ^{13}c Phospholactate. *J. Am. Chem. Soc.* **2012**, *134*, 3957−3960.
(25) Kovtunov, K. V.; Truong, M. L.; Barskiy, D. A.; Koptyug, I. V.; Waddell, K. W.; Chekmenev, E. Y. Long-Lived Spin States for Low-Field Hyperpolarized Gas MRI. *Chem.—Eur. J.* **2014**, *20*, 14629−14632.
(26) George, Z. M.; Habgood, H. W. Mechanism of Hydrogen-Deuterium Exchange of Propylene over a Bronsted Zeolite Catalyst. *J. Phys. Chem.* **1972**, *76*, 3940−3943.
(27) Kubelkova, L.; Novakova, J.; Jiru, P. Exchange of Propene-D-6 with Hydrogen of HY Zeolites. *React. Kinet. Catal. Lett.* **1976**, *4*, 151−157.
(28) Coffey, A. M.; Truong, M. L.; Chekmenev, E. Y. Low-Field MRI Can Be More Sensitive Than High-Field MRI. *J. Magn. Reson.* **2013**, *237*, 169−174.
(29) Hayden, M. E.; Bidinosti, C. P.; Chapple, E. M. Specific Absorption Rates and Signal-to-Noise Ratio Limitations for MRI in Very-Low Magnetic Fields. *Concept Magn. Reson. A* **2012**, *40A*, 281−294.
(30) McKee, R. H.; Herron, D.; Saperstein, M.; Podhasky, P.; Hoffman, G. M.; Roberts, L. The Toxicological Properties of Petroleum Gases. *Int. J. Toxicol.* **2014**, *33*, 28S−51S.
(31) Feng, B.; Coffey, A. M.; Colon, R. D.; Chekmenev, E. Y.; Waddell, K. W. A Pulsed Injection Parahydrogen Generator and Techniques for Quantifying Enrichment. *J. Magn. Reson.* **2012**, *214*, 258−262.
(32) Waddell, K. W.; Coffey, A. M.; Chekmenev, E. Y. In Situ Detection of PHIP at 48 mT: Demonstration Using a Centrally Controlled Polarizer. *J. Am. Chem. Soc.* **2011**, *133*, 97−101.
(33) Coffey, A. M.; Shchepin, R. V.; Wilkens, K.; Waddell, K. W.; Chekmenev, E. Y. A Large Volume Double Channel ^{1}H-X Rf Probe for Hyperpolarized Magnetic Resonance at 0.0475 T. *J. Magn. Reson.* **2012**, *220*, 94−101.
(34) Pravica, M. G.; Weitekamp, D. P. Net NMR Alignment by Adiabatic Transport of Parahydrogen Addition Products to High Magnetic Field. *Chem. Phys. Lett.* **1988**, *145*, 255−258.
(35) Bowers, C. R.; Weitekamp, D. P. Para-Hydrogen and Synthesis Allow Dramatically Enhanced Nuclear Alignment. *J. Am. Chem. Soc.* **1987**, *109*, 5541−5542.
(36) De Coene, B.; Hajnal, J. V.; Gatehouse, P.; Longmore, D. B.; White, S. J.; Oatridge, A.; Pennock, J. M.; Young, I. R.; Bydder, G. M. MR of the Brain Using Fluid-Attenuated Inversion Recovery (FLAIR) Pulse Sequences. *Am. J. Neuroradiol.* **1992**, *13*, 1555−64.
(37) Nikolaou, P.; Coffey, A. M.; Walkup, L. L.; Gust, B. M.; Whiting, N.; Newton, H.; Barcus, S.; Muradyan, I.; Dabaghyan, M.; Moroz, G. D.; et al. Near-Unity Nuclear Polarization with an 'Open-Source' ^{129}Xe Hyperpolarizer for NMR and MRI. *Proc. Natl. Acad. Sci. U.S.A.* **2013**, *110*, 14150−14155.
(38) Weiger, M.; Pruessmann, K. P.; Bracher, A.-K.; Köhler, S.; Lehmann, V.; Wolfram, U.; Hennel, F.; Rasche, V. High-Resolution ZTE Imaging of Human Teeth. *NMR Biomed.* **2012**, *25*, 1144−1151.
(39) Barskiy, D. A.; Kovtunov, K. V.; Primo, A.; Corma, A.; Kaptein, R.; Koptyug, I. V. Selective Hydrogenation of 1,3-Butadiene and 1-Butyne over a Rh/Chitosan Catalyst Investigated by Using Para-hydrogen-Induced Polarization. *ChemCatChem.* **2012**, *4*, 2031−2035.
(40) Kovtunov, K. V.; Beck, I. E.; Zhivonitko, V. V.; Barskiy, D. A.; Bukhtiyarov, V. I.; Koptyug, I. V. Heterogeneous Addition of H-2 to Double and Triple Bonds over Supported Pd Catalysts: A Para-hydrogen-Induced Polarization Technique Study. *Phys. Chem. Chem. Phys.* **2012**, *14*, 11008−11014.
(41) Meriles, C. A.; Sakellariou, D.; Trabesinger, A. H.; Demas, V.; Pines, A. Zero- to Low-Field MRI with Averaging of Concomitant Gradient Fields. *Proc. Natl. Acad. Sci. U.S.A.* **2005**, *102*, 1840−1842.
(42) Appelt, S.; Kuhn, H.; Hasing, F. W.; Blumich, B. Chemical Analysis by Ultrahigh-Resolution Nuclear Magnetic Resonance in the Earths Magnetic Field. *Nat. Phys.* **2006**, *2*, 105−109.
(43) Ruset, I. C.; Tsai, L. L.; Mair, R. W.; Patz, S.; Hrovat, M. I.; Rosen, M. S.; Muradian, I.; Ng, J.; Topulos, G. P.; Butler, J. P.; et al. A System for Open-Access He-3 Human Lung Imaging at Very Low Field. *Concept Magn. Reson. B* **2006**, *29B*, 210−221.
(44) Nikolaou, P.; Coffey, A. M.; Ranta, K.; Walkup, L. L.; Gust, B.; Barlow, M. J.; Rosen, M. S.; Goodson, B. M.; Chekmenev, E. Y. Multi-Dimensional Mapping of Spin-Exchange Optical Pumping in Clinical-Scale Batch-Mode ^{129}Xe Hyperpolarizers. *J. Phys. Chem. B* **2014**, *118*, 4809−4816.
(45) Goldman, M.; Johannesson, H.; Axelsson, O.; Karlsson, M. Hyperpolarization of C-13 through Order Transfer from Para-hydrogen: A New Contrast Agent for MFI. *Magn. Reson. Imaging* **2005**, *23*, 153−157.
(46) Bhattacharya, P.; Chekmenev, E. Y.; Reynolds, W. F.; Wagner, S.; Zacharias, N.; Chan, H. R.; Bünger, R.; Ross, B. D. Parahydrogen-Induced Polarization (PHIP) Hyperpolarized MR Receptor Imaging in Vivo: A Pilot Study of ^{13}C Imaging of Atheroma in Mice. *NMR Biomed.* **2011**, *24*, 1023−1028.
(47) Bhattacharya, P.; Chekmenev, E. Y.; Perman, W. H.; Harris, K. C.; Lin, A. P.; Norton, V. A.; Tan, C. T.; Ross, B. D.; Weitekamp, D. P. Towards Hyperpolarized ^{13}C-Succinate Imaging of Brain Cancer. *J. Magn. Reson.* **2007**, *186*, 150−155.
(48) Chekmenev, E. Y.; Hovener, J.; Norton, V. A.; Harris, K.; Batchelder, L. S.; Bhattacharya, P.; Ross, B. D.; Weitekamp, D. P. PASADENA Hyperpolarization of Succinic Acid for MRI and NMR Spectroscopy. *J. Am. Chem. Soc.* **2008**, *130*, 4212−4213.
(49) Zacharias, N. M.; Chan, H. R.; Sailasuta, N.; Ross, B. D.; Bhattacharya, P. Real-Time Molecular Imaging of Tricarboxylic Acid Cycle Metabolism in Vivo by Hyperpolarized 1-C-13 Diethyl Succinate. *J. Am. Chem. Soc.* **2012**, *134*, 934−943.
(50) Shchepin, R. V.; Pham, W.; Chekmenev, E. Y. Dephosphorylation and Biodistribution of 1-^{13}C-Phospholactate in Vivo. *J. Labelled Compd. Radiopharm.* **2014**, *57*, 517−524.
(51) Reineri, F.; Viale, A.; Ellena, S.; Alberti, D.; Boi, T.; Giovenzana, G. B.; Gobetto, R.; Premkumar, S. S. D.; Aime, S. N-15 Magnetic Resonance Hyperpolarization Via the Reaction of Parahydrogen with N-15-Propargylcholine. *J. Am. Chem. Soc.* **2012**, *134*, 11146−11152.
(52) Goldman, M.; Johannesson, H. Conversion of a Proton Pair Para Order into C-13 Polarization by Rf Irradiation, for Use in MRI. *C. R. Phys.* **2005**, *6*, 575−581.
(53) Cai, C.; Coffey, A. M.; Shchepin, R. V.; Chekmenev, E. Y.; Waddell, K. W. Efficient Transformation of Parahydrogen Spin Order into Heteronuclear Magnetization. *J. Phys. Chem. B* **2013**, *117*, 1219−1224.
(54) Kadlecek, S.; Vahdat, V.; Nakayama, T.; Ng, D.; Emami, K.; Rizi, R. A Simple and Low-Cost Device for Generating Hyperpolarized Contrast Agents Using Parahydrogen. *NMR Biomed.* **2011**, *24*, 933−942.
(55) Baer, S.; Lange, T.; Leibfritz, D.; Hennig, J.; von Elverfeldt, D.; Hoevener, J.-B. On the Spin Order Transfer from Parahydrogen to Another Nucleus. *J. Magn. Reson.* **2012**, *225*, 25−35.
(56) Carravetta, M.; Levitt, M. H. Long-Lived Nuclear Spin States in High-Field Solution Nmr. *J. Am. Chem. Soc.* **2004**, *126*, 6228−6229.
(57) Pileio, G.; Carravetta, M.; Hughes, E.; Levitt, M. H. The Long-Lived Nuclear Singlet State of ^{15}N-Nitrous Oxide in Solution. *J. Am. Chem. Soc.* **2008**, *130*, 12582−12583.
(58) Warren, W. S.; Jenista, E.; Branca, R. T.; Chen, X. Increasing Hyperpolarized Spin Lifetimes through True Singlet Eigenstates. *Science* **2009**, *323*, 1711−1714.
(59) Theis, T.; Feng, Y.; Wu, T.; Warren, W. S. Composite and Shaped Pulses for Efficient and Robust Pumping of Disconnected Eigenstates in Magnetic Resonance. *J. Chem. Phys.* **2014**, *140*, 7.

(60) Zhang, Y. N.; Soon, P. C.; Jerschow, A.; Canary, J. W. Long-Lived ^{1}H Nuclear Spin Singlet in Dimethyl Maleate Revealed by Addition of Thiols. *Angew. Chem., Int. Ed.* **2014**, *53*, 3396−3399.
(61) Hughes-Riley, T.; Six, J. S.; Lilburn, D. M. L.; Stupic, K. F.; Dorkes, A. C.; Shaw, D. E.; Pavlovskaya, G. E.; Meersmann, T. Cryogenics Free Production of Hyperpolarized ^{129}Xe and ^{83}Kr for Biomedical MRI Applications. *J. Magn. Reson.* **2013**, *237*, 23−33.
(62) Tsai, L. L.; Mair, R. W.; Rosen, M. S.; Patz, S.; Walsworth, R. L. An Open-Access, Very-Low-Field MRI System for Posture-Dependent He-3 Human Lung Imaging. *J. Magn. Reson.* **2008**, *193*, 274−285.
(63) Mishkovsky, M.; Cheng, T.; Comment, A.; Gruetter, R. Localized in Vivo Hyperpolarization Transfer Sequences. *Magn. Reson. Med.* **2012**, *68*, 349−352.
(64) Truong, M. L.; Coffey, A. M.; Shchepin, R. V.; Waddell, K. W.; Chekmenev, E. Y. Sub-Second Proton Imaging of ^{13}C Hyperpolarized Contrast Agents in Water. *Contrast Media Mol. Imaging* **2014**, *9*, 333−341.
(65) Kovtunov, K. V.; Barskiy, D.; Shchepin, R. V.; Coffey, A. M.; Waddell, K. W.; Koptyug, I. V.; Chekmenev, E. Y. Demonstration of Heterogeneous Parahydrogen Induced Polarization Using Hyperpolarized Agent Migration from Dissolved Rh(I) Complex to Gas Phase. *Anal. Chem.* **2014**, *86*, 6192−6196.
(66) Nikolaou, P.; Coffey, A. M.; Walkup, L. L.; Gust, B.; LaPierre, C.; Koehnemann, E.; Barlow, M. J.; Rosen, M. S.; Goodson, B. M.; Chekmenev, E. Y. A 3D-Printed High Power Nuclear Spin Polarizer. *J. Am. Chem. Soc.* **2014**, *136*, 1636−1642.
(67) Nikolaou, P.; Coffey, A. M.; Walkup, L. L.; Gust, B. M.; Whiting, N. R.; Newton, H.; Muradyan, I.; Dabaghyan, M.; Ranta, K.; Moroz, G.; et al. XENA: An Automated 'Open-Source' ^{129}Xe Hyperpolarizer for Clinical Use. *Magn. Reson. Imaging* **2014**, *32*, 541−550.
(68) Ruset, I. C.; Ketel, S.; Hersman, F. W. Optical Pumping System Design for Large Production of Hyperpolarized Xe-129. *Phys. Rev. Lett.* **2006**, *96*, 053002.
(69) Zook, A. L.; Adhyaru, B. B.; Bowers, C. R. High Capacity Production of > 65% Spin Polarized Xenon-129 for NMR Spectroscopy and Imaging. *J. Magn. Reson.* **2002**, *159*, 175−182.
(70) Walkup, L. L.; Woods, J. C. Translational Applications of Hyperpolarized ^{3}He and ^{129}Xe. *NMR Biomed.* **2014**, DOI: 10.1002/nbm.3151.
(71) Kurhanewicz, J.; Vigneron, D. B.; Brindle, K.; Chekmenev, E. Y.; Comment, A.; Cunningham, C. H.; DeBerardinis, R. J.; Green, G. G.; Leach, M. O.; Rajan, S. S.; et al. Analysis of Cancer Metabolism by Imaging Hyperpolarized Nuclei: Prospects for Translation to Clinical Research. *Neoplasia* **2011**, *13*, 81−97.
(72) Nikolaou, P.; Goodson, B. M.; Chekmenev, E. Y. NMR Hyperpolarization Techniques for Biomedicine. *Chem.—Eur. J.* **2014**, DOI: 10.1002/chem.201405253.
(73) Sarracanie, M.; Armstrong, B. D.; Stockmann, J.; Rosen, M. S. High Speed 3D Overhauser-Enhanced MRI Using Combined B-Ssfp and Compressed Sensing. *Magn. Reson. Med.* **2014**, *71*, 735−745.
(74) Dominguez-Viqueira, W.; Berger, W.; Parra-Robles, J.; Santyr, G. E. Litz Wire Radiofrequency Receive Coils for Hyperpolarized Noble Gas MR Imaging of Rodent Lungs at 73.5 mT. *Concept Magn. Reson. B* **2010**, *37B*, 75−85.